Hunting for QCD Instantons at the LHC in Events with Large Rapidity Gaps

V. A. Khoze[a,b], V. V. Khoze[b], D. L. Milne[b] and M. G. Ryskin[a,b]

[a] Petersburg Nuclear Physics Institute, NRC Kurchatov Institute, Gatchina,
St. Petersburg, 188300, Russia
[b] IPPP, Department of Physics, Durham University, Durham, DH1 3LE, UK

Abstract

We outline a strategy of how to search for QCD instantons of invariant mass $20 - 60$ GeV in diffractive events in low luminosity runs at the LHC. We show that by imposing appropriate selection criteria on the final states, one can select the kinematic regime where the instanton signal exceeds the background by a factor of at least 2.5. In spite of the relatively strong cuts that we impose on the total transverse energy and the number of charged tracks, $\sum_i E_{T,i} > 20$ GeV, $N_{\mathrm{ch}} > 20$ measured within the $0 < \eta < 2$ interval, the expected cross-section is sufficiently large to study the instanton production in the events with Large Rapidity Gaps at low luminosities, thus avoiding problems with pile-up. The paper also includes an updated computation of instanton cross-sections and other parameters relevant for the ongoing studies.

E-mail: `v.a.khoze@durham.ac.uk`, `valya.khoze@durham.ac.uk`,
`daniel.l.milne@durham.ac.uk`, `ryskin@thd.pnpi.spb.ru`

1 Introduction

Instantons are non-perturbative classical solutions of Euclidean equations of motion in non-abelian gauge theories [1]. In the semi-classical limit, instantons provide dominant contributions to the path integral and describe quantum tunnelling between different vacuum sectors of the theory [2, 3, 4]. Over the years a number of phenomenological models and approaches were developed where QCD instantons were either directly responsible for generating, or at least contributed to many key aspects of non-perturbative low-energy dynamics of strong interactions [5, 6, 7, 8, 9, 10]. These include the role of instantons in the breaking of the $U(1)_A$ symmetry and the spontaneous breakdown of the chiral symmetry, the formation of quark and gluon condensates, topological susceptibility of the vacuum, and the non-perturbative generation of the axion potential. Instanton-based phenomenological models provide at least a qualitative description of the QCD vacuum.[1] These predictions are in good agreement with lattice calculations [11], see also [12, 13].

Our motivation here is different. We would like to search for QCD instanton events directly in scattering experiments. This setup provides a more controlled environment than QCD vacuum modelling, as the scattering event kinematics will enable us to remain in a relatively weakly-coupled regime where semiclassical instanton methods are reliable. In scattering processes the instanton can be thought of as new non-perturbative multi-particle vertices in a Feynman diagram, and for its computation at the microscopic level we will use the formalism developed in the recent papers [14, 15]. QCD instanton-generated processes are predicted to be produced with a large scattering cross-section at small centre-of-mass partonic energies, although, as shown in [15], discovering them at hadron colliders using conventional high-p_T trigger requirements, is a challenging task that requires alternative dedicated search strategies. Developing such a strategy based on the event selection with large rapidity gaps at low luminosities is the purpose of this paper.

In the past, in the context of deep inelastic scattering, QCD instanton contributions [16, 17, 18] were searched for (but not observed) [19, 20] at the HERA collider.

---

[1]Their potential short-comings originate from attempting to describe the strongly-coupled QCD vacuum dynamics using a semi-classical (weak-coupling) approximation where the path integral is expanded around classical instanton background fields.

In QCD, the instanton configuration consists of the gauge field,

$$A_\mu^{a\,\text{inst}}(x) = \frac{2\rho^2}{g} \frac{\bar\eta_{\mu\nu}^a (x-x_0)_\nu}{(x-x_0)^2((x-x_0)^2 + \rho^2)}\,, \tag{1}$$

along with the fermion components for light ($m_f < 1/\rho$) fermions,

$$\bar q_{Lf} = \psi^{(0)}(x)\,, \quad q_{Rf} = \psi^{(0)}(x)\,. \tag{2}$$

The gauge field $A_\mu^{a\,\text{inst}}$ is the Belavin-Polyakov-Schwartz-Tyupkin (BPST) instanton solution [1] of the self-duality equations in the singular gauge. Here ρ is the instanton size and x_0 is the instanton position. Constant group-theoretic coefficients $\bar\eta_{\mu\nu}^a$ are the 't Hooft eta symbols defined in [2]. The fermionic components $\psi^{(0)}$ are the corresponding normalised solutions of the Dirac equation $\gamma^\mu D_\mu[A_\mu^{a\,\text{inst}}]\psi^{(0)} = 0$. These are the fermion zero modes of the instanton. The instanton configuration is a local minimum of the Euclidean action, and the action on the instanton is given by $S_I = \frac{8\pi^2}{g^2} = \frac{2\pi}{\alpha_s}$.

The instanton configuration (1) has topological charge equal to one and thus, due to the chiral anomaly, the instanton processes violate chirality. If the instanton is produced by a two-gluon initial state, the final state of this instanton-mediated process will have N_f pairs of quarks and anti-quarks with the same chirality,

$$g + g \to n_g \times g + \sum_{f=1}^{N_f}(q_{Rf} + \bar q_{Lf})\,, \tag{3}$$

where N_f is the number of light flavours relative to the inverse instanton size, $m_f < 1/\rho$. The instanton contribution to the amplitude for this process comes from expanding the corresponding path integral in the instanton field background. At leading order in the instanton perturbation theory, the amplitude takes the form of an integral over the instanton collective coordinates (see e.g. Refs. [14, 15] for more detail),

$$\mathcal{A}_{2\to n_g+2N_f}^{\text{L.O.}} = \int d^4 x_0 \int_0^\infty d\rho\, D(\rho)\, e^{-S_I} \prod_{i=1}^{n_g+2} A_{\text{LSZ}}^{\text{inst}}(p_i;\rho) \prod_{j=1}^{2N_f} \psi_{\text{LSZ}}^{(0)}(p_j;\rho). \tag{4}$$

The factors of $A_{\text{LSZ}}^{\text{inst}}(p_i;\rho)$ and $\psi_{\text{LSZ}}^{(0)}(p_j;\rho)$ are the standard insertions of the LSZ-reduced instanton fields in the momentum representation and $D(\rho)$ is given by the known expression for the instanton density [2].

3

From the point of view of Feynman graphs the leading order instanton amplitude (4) reveals itself as a family of multi-particle vertices (with different numbers of emitted gluons) integrated over the instanton position and size. It describes the emission of a large number of gluons, $n_g \propto E^2/\alpha_s$, together with a fixed number of quarks and anti-quarks, one pair for each light flavour in accordance with (3). The semi-classical suppression factor, $\exp(-S_I) = \exp(-2\pi/\alpha_s)$, will be partially compensated by the growth with jet energy, E, of the high multiplicity cross-section for the process (3). The fully factorised structure of the field insertions on the right hand side of (4) implies that at leading order in instanton perturbation theory there are no correlations between the momenta of the external legs in the instanton amplitude. The momenta of individual particles in the final state are mutually independent, apart from overall momentum conservation.

Thus to discover the QCD instanton we have to observe in the final state a multi-particle cluster or a fireball which contains in general a large number of isotropically distributed gluon (mini)jets accompanied by N_f pairs of light quark jets generated by a subprocess such as (3).

It is quite challenging, however, to identify the instanton on top of the underlying event. Recall that the instanton is not a particle and there will be no peak in the invariant mass, M_{inst}, distribution [2]. The mean value of M_{inst} can at least in principle be "measured" or reconstructed as the mass of the minjet system created by the instanton fireball in each given event. Talking about the instanton we actually mean a family of objects of different sizes, ρ and different orientation in the colour and the Lorentz spaces. The mean value of M_{inst} depends on ρ, increasing when ρ decreases. Since experimentally it is impossible to measure the instanton size, ρ, below we use the mass M_{inst} to characterise the properties of the instanton production event.

The paper is organised as follows; in Section 2 we detail the main sources of background and how their cross-section behaves with energy. Section 3 details the physics of events with large rapidity gaps while Section 4 explains the rationale behind the selection criteria employed in this paper. Section 5 updates the calculation of cross-sections presented in [15] to account for small virtualities present in incoming gluons and provides details of the Monte

---

[2]What we mean by the instanton mass is the partonic energy $\sqrt{\hat{s}}$ of the initial 2-gluon state in the process (3). As we integrate over the Bjorken x variables when computing hadronic cross-section, we sum over a broad range of instanton masses.

Carlo generation of our background. In Section 6 we give our results and Section 7 provides a discussion theoretical uncertainties and additional instanton sub-processes. In section 8 we present our conclusions.

2   Background

Let us consider the main sources of background which can mimic the instanton signal.

The cross-section of instanton production falls steeply with M_{inst} mainly due to the factor $\exp(-S_I) = \exp(-2\pi/\alpha_s(\rho))$ in the amplitude. At smaller values of ρ the instanton action $S_I = 2\pi/\alpha_s(\rho)$ increases since the QCD coupling α_s decreases. Calculations presented in Section 5 (*cf.* Table 1) show that the elementary cross-section of the parton level subprocess (3) falls approximately as

$$\hat{\sigma}_{\text{inst}} \propto M_{\text{inst}}^{-6} , \qquad (5)$$

over a broad low-to-intermediate energy range (it becomes less steep, $\hat{\sigma}_{\text{inst}} \propto M_{\text{inst}}^{-4}$, at lower energies $20-30$ GeV).

On the other hand the dimensionless rate, $M^2 \sigma_{\text{pQCD}}$, of a similar purely perturbative QCD subprocess, $gg \to N$minijets, decreases only logarithmically. For the perturbatively formed 'hedgehog' configuration of N final state jets we would expect

$$\sigma_{\text{pQCD}}(gg \to N \, \text{jets}) \sim \frac{16\pi}{M^2} \left(\frac{N_c}{\pi} \alpha_s(M) \right)^N , \qquad (6)$$

where M denotes the invariant energy of the perturbatively formed cluster of minijets. Thus, at sufficiently large values of M_{inst} the instanton signal (5) will become negligible relative to the purely perturbative QCD production (6).

In the regime of interest of moderately small M_{inst} we face however another problem that needs to be addressed. The instanton event can be mimicked by the multiple parton interactions (MPI) illustrated in Fig. 1. Indeed, the double (triple, ..., n) parton scattering produces a few pairs of jets (dijets) which would look like a fireball, thus obscuring the final state signature of the genuine instanton signal.
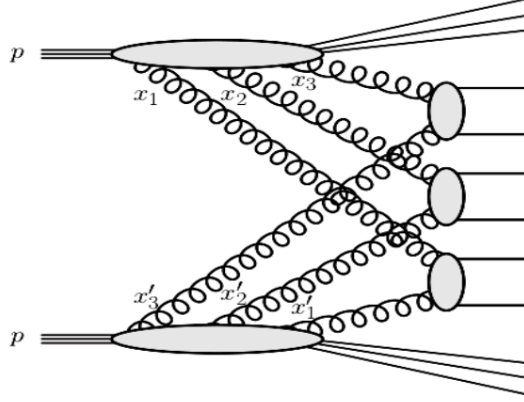
Figure 1: Schematic diagram for the triple parton scattering process.

The cross-section of such a process can be evaluated as

$$\frac{d\sigma}{dE_1^2...dE_n^2} \sim \left(\frac{d\sigma}{\sigma_{eff}dE_1^2} \; ... \; \frac{d\sigma}{\sigma_{eff}dE_n^2} \right) \sigma_{eff} \; , \tag{7}$$

where E_i denotes the transverse energy of a jet in the i dijet system, $\sigma_{eff} \sim$ 10 mb (see Fig. 4 of [21] and references therein) and the cross section $d\sigma/dE_i^2 \sim \pi\alpha_s^2/E_i^4$. That is, at low M_{inst} when the transverse energies of produced jets become small, the MPI processes will dominate. It was shown in [22] that the events caused by such multiple parton interactions manifest high sphericity S, similar to the instanton signal. Our strategy to suppress them is outlined in the following section and involves a final state selection with Large Rapidity Gaps.

Finally, we would like to emphasise one additional point. Since our knowledge on the dynamics of confinement and hadronization is quite limited, general purpose Monte Carlo (MC) event generators introduce certain phenomenological parameters that are tuned in order to better describe the experimental data (for a review see e.g. Ref. [23]). But if a low-mass instanton contributes to the scattering, its presence will affect the data, and after such tuning we lose the possibility to distinguish the low M_{inst} instanton from other hadronization effects.

3   Events with Large Rapidity Gaps

As discussed above, we expect a large 'underlying event' background both in the region of large and small instanton masses. However the low M_{inst} background caused by multi-parton interactions can be effectively suppressed by selecting events with Large Rapidity Gaps (LRG). Indeed, each additional 'parton-parton$\rightarrow$ dijet' scattering is accompanied by the colour flow created by the parton cascade needed to form the incoming partons (see Fig. 1). This colour flow produces secondaries which fill the LRG. The LRG survival probability, S^2, (i.e. the probability not to destroy the LRG) is rather small, $S^2 \leq 0.1$, see e.g. [24]. Thus the probability to observe n additional branches of parton-parton interactions in LRG events is suppressed by the factor $(S^2)^n$.

Moreover, recall that the events with an LRG mainly occur at large values of b_t, (the separation between the two incoming protons in the transverse plane), where the proton optical density (opacity) is small [24, 25]. On the other hand, the MPI (Double/Triple/.../n Parton Scattering) processes proceed dominantly at small values of b_t, where the proton opacity is much larger. Thus, we expect that the suppression factor, S^2, for each additional scattering should be smaller than the average value of S^2 discussed in [24]. Therefore in this paper when evaluating backgrounds for relatively low mass instantons in the events with an LRG, to a first approximation we neglect the MPI/nPS contributions.

4   Search strategy

We propose searching for the instanton as a multi-particle cluster/fireball with a mass of about 20 – 60 GeV in the events with an LRG. The presence of an LRG can be detected either by detecting the leading forward proton with beam momentum fraction, $x_L = 1-\xi$, very close to 1 ($\xi = x_{Pom} \leq 0.01$), or by observing no hadron activity in the forward calorimeters.

Since the relatively heavy instanton produces a rather large number of jets we are looking for high multiplicity events which:

- do not contain high-E_T jets, and
- still have a large density of the transverse energy, $\sum_i dE_{Ti}/d\eta \sim M_{\text{inst}}/3$ (the sum is over all secondary particles in the given η interval).

Indeed, from Table 1 we see that the instanton of mass 30 GeV produces about 17 jets (9 gluons plus 4 light $\bar{q}q$ pairs). The energy of each jet $E_{Ti} \sim 1/\rho \sim 2$ GeV. After hadronization in such an event we expect about 40-60 particles. The large multiplicity can be used as the main (or additional) trigger to select the events of interest.

Note that the elementary (parton level) instanton cross-section is predicted to be rather large ($\sim 1\mu b$) while the background due to hedgehog-like pQCD multijet production (6) is much smaller – already for the case of 6 final jets the expected elementary (hedgehog QCD) cross-section $\sim$ few·nb which can be safely neglected.

On the other hand, in the events with an LRG, the probability to observe such large multiplicity in a limited rapidity interval falls steeply with N_{track} (see e.g. Fig. 13 of [25]). Moreover, since each jet from the instanton cluster contains a leading hadron with $p_T \geq 1$ GeV, we can select the events with a large multiplicity (say, $N_{ch}(p_T > 0.5\text{GeV}) > 20$) of high p_T particles, in this way strongly suppressing the soft QCD background.

Since the LHC detectors never cover the whole (4π) rapidity interval, there is no chance to adequately measure the value of M_{inst}. To select the events with appropriate M_{inst} we introduce the cut on the total transverse energy measured within the given rapidity interval $\sum_i E_{Ti} > M_0$.

Here we consider the instanton production in the pomeron-proton collision (in terms of Regge theory the pomeron exchange is responsible for the presence of the LRG) selecting events with a large multiplicity and relatively large transverse energy [3]. We expect that these events will be more or less spherically symmetric, that is, in such events there should be a large probability to observe the sphericity S close to 1. Since we can not observe the particles in the whole 4π sphere we consider the "transverse sphericity" (or cylindricity) defined as $S_T = 2\lambda_2/(\lambda_1 + \lambda_2)$ where λ_i are the eigenvalues of the matrix

$$S^{\alpha\beta} = \frac{\sum_i p_i^\alpha p_i^\beta}{\sum_i |\vec{p_i^2}|} \ , \tag{8}$$

and $\lambda_2 < \lambda_1$. Here p_i^α is the two-dimensional transverse component of the

---

[3]The idea to search for the instanton in events with very large multiplicity but not too large transverse energy and the first evaluation of the instanton cross-section at collider energies was discussed long ago in [26].
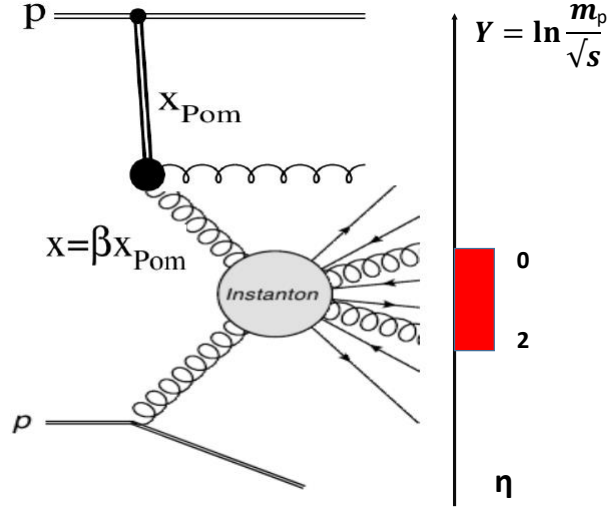
Figure 2: Instanton production in a diffractive process with an LRG. The pomeron exchange is shown by the thick doubled line. The red bar shows the range of η considered in this paper. Y indicates the incoming proton position in rapidity. As shown in the diagram secondaries will be produced outside this range but will not be used when calculating E_T or N_{ch}.

momentum of the i-th particle and we sum over all particles observed in the event within a given rapidity interval.

Finally recall that the decay of the instanton produces one additional pair of each flavour of light $(m_f < 1/\rho)$ quark. So in the case of the signal we expect to observe a larger number of strange and charm particles than in background events.

9

5 Calculation

5.1 Parton-level instanton cross-sections

The instanton cross-sections of the elementary gluon-initiated process (3) are calculated following the approach developed in the recent papers [14, 15]. In this approach the total parton-level instanton cross-section for the process $gg \to X$ is related by the optical theorem to the imaginary part of the forward elastic scattering amplitude computed in the background of the instanton–anti-instanton $(I\bar{I})$ configuration,

$$\hat{\sigma}_{\text{inst}} = \frac{1}{E^2} \operatorname{Im} \mathcal{A}_4^{I\bar{I}}(p_1, p_2, -p_1, -p_2). \tag{9}$$

Here $E = \sqrt{(p_1 + p_2)^2}$ denotes the invariant mass $\sqrt{\hat{s}}$ of the 2-gluon initial state. The resulting instanton cross-section takes the form of the finite-dimensional integral [15] over the instanton and anti-instanton collective coordinates (scale-sizes, ρ and $\bar{\rho}$, the separation between the instanton and anti-instanton centres, R, and the relative $I\bar{I}$ orientations, Ω):

$$\hat{\sigma}_{\text{tot}}^{\text{inst}} \simeq \frac{1}{E^2} \operatorname{Im} \frac{\kappa^2 \pi^4}{36 \cdot 4} \int \frac{d\rho}{\rho^5} \int \frac{d\bar{\rho}}{\bar{\rho}^5} \int d^4 R \int d\Omega \left(\frac{2\pi}{\alpha_s(\mu_r)} \right)^{14} (\rho^2 E)^2 (\bar{\rho}^2 E)^2 \mathcal{K}_{\text{ferm}}(z)$$

$$(\rho\bar{\rho}\mu_r^2)^{b_0} \exp\left(R_0 E - \frac{4\pi}{\alpha_s(\mu_r)} \mathcal{S}(z) - \frac{\alpha_s(\mu_r)}{16\pi}(\rho^2 + \bar{\rho}^2) E^2 \log \frac{E^2}{\mu_r^2} - Q(\rho + \bar{\rho}) \right). \tag{10}$$

In the above integral κ^2 denotes the known normalization constant and $\mathcal{K}_{\text{ferm}}(z)$ is the factor arising from the overlap of fermion zero modes of I and $\bar{I}$ and the variable z is a certain conformally-invariant ratio of the collective coordinates R, ρ and $\bar{\rho}$ [27, 28],

$$z = \frac{R^2 + \rho^2 + \bar{\rho}^2 + \sqrt{(R^2 + \rho^2 + \bar{\rho}^2)^2 - 4\rho^2\bar{\rho}^2}}{2\rho\bar{\rho}}. \tag{11}$$

The first factor in the exponent in (10) describes the energy input from the initial state, the second factor is the action of the instanton-anti-instanton configuration [28], $S_{I\bar{I}}(z) = \frac{4\pi}{\alpha_s} \mathcal{S}(z)$ where,

$$\mathcal{S}(z) = 3\frac{6z^2 - 14}{(z - 1/z)^2} - 17 - 3\log(z) \left(\frac{(z - 5/z)(z + 1/z)^2}{(z - 1/z)^3} - 1 \right). \tag{12}$$

The third term in the exponent,

$$\exp\left(-\frac{\alpha_s(\mu_r)}{16\pi}\left(\rho^2+\bar{\rho}^2\right)E^2\,\log\frac{E^2}{\mu_r^2}\right),\tag{13}$$

is the quantum effect that takes into account resummed perturbative exchanges between the hard initial state gluons and the instantons [29]. Inclusion of these quantum effects is required in order to resolve the well-known infra-red problem in the $\rho, \bar{\rho} \to \infty$ limit, as QCD instantons with $\rho \gg \left(\frac{16\pi}{\alpha_s}\frac{1}{E^2\log E^2}\right)^{1/2}$ are automatically cut-off by these quantum corrections.

We note that the initial-state partons (in our case gluons) are not strictly on mass-shell, but carry small order-GeV virtualities, Q_1 and Q_2. For the gluon emitted from the pomeron we choose $Q_1 = 2$ GeV, and the second gluon that originated from the proton has the virtuality $Q_2 = 1$ GeV. [4] These virtualities introduce the form-factor[5] $e^{-Q\rho}$ in the instanton vertex, with $Q = Q_1 + Q_2 = 3$ GeV in our case. This is the origin of the final term,

$$\exp\left(-Q(\rho+\bar{\rho})\right),\tag{14}$$

in the exponent of the cross-section in (10).

To further simplify the integrand we select a natural value for the renormalization scale dictated by the inverse instanton size. This prescription removes the large $(\rho\mu_r)^{b_0}(\bar{\rho}\mu_r)^{b_0}$ factor in front of the exponent in (10). Hence we choose,

$$\mu_r = 1/\langle\rho\rangle = 1/\sqrt{\rho\bar{\rho}}.\tag{15}$$

For the reference point of α_s we choose its value at the τ mass, $\alpha_s(m_\tau) = 0.32$ following [31, 32] that fits the experimental data [33, 34]. The choice of

---

[4]From the pomeron side the expected virtuality $Q_1^2 \simeq q_t^2$ is close to the mean transverse momentum squared, q_t^2, of the gluon inside the pomeron. Its value can be estimated as $q_t^2 \sim 1/\alpha'_P \sim 4$ GeV^2 where we take the pomeron trajectory slope $\alpha'_p = 0.25$ GeV^{-2} [30]. The gluon virtuality in the proton PDF, $Q_2 \sim 1$ GeV was chosen for the following reasons. As a rule the global parton analysis based on DGLAP evolution starts the evolution at some $Q = Q_0 \geq 1$ GeV. We do not know the parton distributions at a smaller Q (it is not even clear whether we can use the parton language at such small Q). Note however that the low-x gluon density increases as the scale Q increases. So we consider the value of $Q_2 = 1$ GeV as a conservative estimate.

[5]The form-factor is a direct consequence of Fourier transforming the instanton field to momentum space to obtain $A_{LSZ}^{\rm inst}(p_i)$, where the momentum p_i has the virtuality, Q_i^2 [28], and was explored and used extensively in the context of deep inelastic scattering in [16, 18].

m_τ as the reference scale for α_s is conveniently close to the interesting (for us) regime of relatively light instantons with sizes $1/\langle\rho\rangle \sim$ few GeV. For the running coupling at energy scales above m_τ, we use the 1-loop expression, while for the lower scales we freeze the coupling at a fixed critical value $\alpha_s = 0.35$,

$$\frac{4\pi}{\alpha_s(\langle\rho\rangle)} \simeq \begin{cases} \frac{4\pi}{0.32} - 2b_0 \log\left(\langle\rho\rangle\, m_\tau\right) & : \text{ for } \langle\rho\rangle^{-1} \geq 1.45\,\text{GeV} \\ \frac{4\pi}{0.35} & : \text{ for } \langle\rho\rangle^{-1} < 1.45\,\text{GeV}\,. \end{cases} \tag{16}$$

At these energy-scales we are in the regime of

$$N_f = 4\,, \tag{17}$$

active quarks, and this is the N_f value we use in $b_0 = 11 - 2N_f/3$ and in the instanton density expressions for κ^2 and $\mathcal{K}_{\text{ferm}}$ in (10).

The rationale for freezing the coupling at 0.35 is that the perturbative evolution of strong coupling at the order ~ 1 GeV scale is known to be in conflict with observations. The strong coupling values extracted from the fits to charmonium spectrum give $\alpha_s \simeq 0.35$ at 1 to 1.2 GeV scale [35], which is close to the measured value $\alpha_s(m_\tau)$ at the considerably higher scale $m_\tau = 1.777$ GeV, and is about 50% below the prediction of the 2-loop perturbative running. These considerations justify freezing the strong coupling in the infrared at a critical value $\alpha_s = 0.35$, the approach we will follow in accordance with (16).

The authors of Ref. [15], evaluated the integral in (10) numerically using the python package SciPy [36] to derive the parton-level instanton cross-sections along with the mean number of gluons in the final state as functions of partonic energy E. In this work we follow the computational approach of [15], except that we now also account for the effect of $Q \simeq 3$ GeV gluon virtualities (14) from the outset, and use the prescription (16) for the running coupling.

The data in Table 1 shows that the instanton production cross-section $\hat{\sigma}_{\text{inst}}$ is sharply suppressed at high partonic energies (high instanton masses) and becomes large at low values of E. This is also consistent with the earlier calculations in [14] that used the same theory set-up for the parton-level instanton cross-section (10), but evaluated the integral in the steepest descent approximation. The sharp suppression of the instanton cross-section at large partonic energies is the consequence of the inclusion of the quantum

E [GeV]	$\hat{\sigma}\,(gg \to I)$ [pb]	$\langle 1/\rho \rangle$ [GeV]	$\alpha_s\,(1/\rho)$	$\langle n_g \rangle$
20	2.01×10^6	1.69	0.327	7.81
25	9.49×10^5	1.98	0.306	8.58
30	4.64×10^5	2.27	0.290	9.07
35	2.32×10^5	2.52	0.279	9.61
40	1.25×10^5	2.84	0.267	9.67
50	3.89×10^4	3.38	0.251	10.56
60	1.38×10^4	3.87	0.241	10.89
70	5.45×10^3	4.33	0.232	11.38
80	2.36×10^3	4.85	0.224	11.67
90	1.08×10^3	5.24	0.219	12.31
100	5.44×10^2	5.82	0.213	12.10
110	2.79×10^2	6.21	0.209	12.62
120	1.53×10^2	6.71	0.205	12.77
130	8.56×10^1	7.13	0.201	13.04
140	4.99×10^1	7.57	0.198	13.25
150	3.01×10^1	8.00	0.195	13.45

Table 1: The instanton production cross-section for the sub-process (3) for a range of partonic cms energies E (i.e. instanton masses) and the mean number of emitted gluons in addition to the mean value of $1/\rho$ and $\alpha_s\,(1/\rho)$. For energies larger than 150 GeV, the suppression coming from the 3 GeV virtuality is fairly negligible and one can use the numbers given in [15]. Note that the mean value of R/ρ was ~1.55 at all energies.

exchanges between the hard initial gluons that resulted in the exponential form-factor (13). It cuts off the (anti)-instanton sizes more and more efficiently when E increases, ultimately leading to the integral being dominated by smaller and smaller instantons, thus exponentially suppressing the overall cross-section, in agreement with the results shown in Table. 1 and Fig. 6 in Ref. [14]. In the low-energy limit, contributions of large instantons with $\rho \gg 1/(3\text{GeV})$ are cut-off by gluon virtualities in (14).

For more detail on the theory formalism leading to (10) and the resulting evaluation of $\hat{\sigma}_{\text{inst}}(E)$ and $\langle n_g \rangle(E)$ we refer the reader to Ref. [15].

5.2 Hadronic cross-sections for signal and background

The cross-section of instanton production in proton-proton collisions reads,

$$\sigma_{pp \to I} = \int_{\hat{s}_{min}}^{s_{pp}} dx_1 dx_2 \quad f\left(x_1, Q_1^2\right) f\left(x_2, Q_2^2\right) \hat{\sigma}_{\text{inst}}\left(E^2 = x_1 x_2 s_{pp}\right), \quad (18)$$

where s_{pp} is the centre-of-mass energy of the hadron collider and $\hat{\sigma}$ is the partonic instanton cross-section. Selecting the events with an LRG or the leading proton we have to replace one parton distribution (PDF), say $f(x_1, Q_1^2)$, which describes the probability to find an appropriate parton (gluon) in the incoming proton, by the so-called diffractive PDF, $f^D(x_1, Q_1^2)$, which describes the corresponding distribution in the pomeron.

The lower limit $\hat{s}_{min}$ in the integral (18) is introduced for technical reasons. Strictly speaking, one is supposed to integrate from $\hat{s}_{min} = 0$ to s_{pp}. However instantons of masses much smaller than 20 GeV are not under theoretical control, the semiclassical dilute instanton approximation becomes invalid for large instantons with $\rho \sim$ GeV, where the theory can no longer be considered weakly-coupled.[6] It is impossible to fix $\hat{s}_{min}$ experimentally, instead we have to choose and impose experimental cuts on final states that will suppress the contribution of the low mass instantons. In practice we will set $\sqrt{\hat{s}_{min}} = 20\,\text{GeV}$ in the integral,[7] and then impose the cuts.

---

[6]Furthermore, when $\rho \gtrsim 0.3\,\text{fm} \sim 1.5\,\text{GeV}^{-1}$ one can no longer distinguish between the instantons created in collisions and the instanton-like configurations populating the QCD ground state [11]. The role of $\hat{s}_{min}$ is to cut-off such large ground-state field configurations.

[7]Taking $\hat{s}_{min} = (20\text{GeV})^2$ gives a hadronic instanton cross-section of 6.78 μb (after multiplying by S^2).

Instanton samples are generated using the RAMBO algorithm [37] and then showered and hadronised using PYTHIA 8 [38]. The scale of the process was taken to be $1/\langle\rho\rangle$ for the purposes of showering in PYTHIA. As already noted, we set the minimum instanton mass generated to be 20 GeV. However we note that the inclusion of these low mass instantons would enhance the signal by no more than 10%.

Background events were simulated by generating inelastic pion-proton collisions (see Fig. 2) in PYTHIA for the proton energy $E_p = 7$ TeV and the pomeron energy $E_{Pom} = 7 \cdot x_{Pom}$ TeV (with a pion being used to simulate a pomeron) and x_{Pom} fixed at 0.003. For the proton PDF we use the NNPDF3.1luxQED NNLO [39, 40, 41, 42] set while for the parton distribution in the pomeron (mimicked in PYTHIA by the pion) the H1 fit B [43] is used. The Q^2 evolution for the pomeron PDF is performed by QCDNUM [44].

When computing the signal, the instanton cross-section calculated in (18) was multipled by the gap survival probabilty, S^2. For simplicity we took $S^2 = 0.1$ in agreement with the experimental results [45, 46] for diffractive high E_T dijet production. The background cross-section was normalised to the experimental yield of single dissociation $d\sigma^{SD}/d\ln(1/x_{Pom}) \simeq 0.15$ mb [47]. In generating both the instanton and the background samples, multi-parton interactions were disabled in PYTHIA.

Since in the case of soft QCD background only a very small fraction of events satisfy the $\sum_i E_{Ti} > M_0$ GeV cut[8] (which we had used further) we generate the "Hard QCD" events with a minimum transverse momentum of 10 GeV using PYTHIA. Using lower p_T samples from PYTHIA, we concluded that the contribution of lower p_T events is negligible.

6 Results

As an example we consider instanton production at 14 TeV in the events with the leading proton momentum fraction $x_L = 1 - x_{Pom} = 0.997$. That is we calculate the cross-section $d\sigma/d\ln(1/x_{Pom})$ at $x_{Pom} = 0.003$. This may be considered as the total observed cross-section when/if one integrates over the

---

[8]Actually to get a large $\sum_i E_{Ti}$ in a perturbative QCD event we have to produce a high E_T jet or to consider the event with a large number of multiple parton interactions. The last possibility is strongly suppressed by the LRG survival factor.
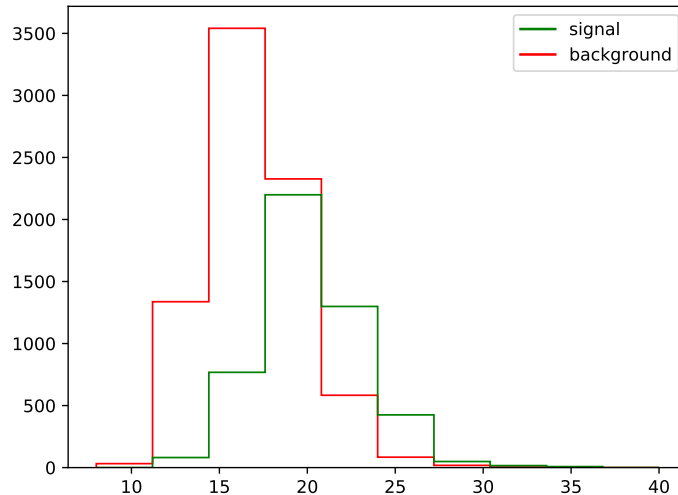
Figure 3: Multiplicity distribution of charged hadrons produced in the events with the instanton (green) in comparison with the expected background (red). Number of events is normalised to the integrated luminosity $L = 1\mathrm{pb}^{-1}$ and $\Delta \ln(x_{Pom}) = 1$ interval. We required events to have $\sum_i E_{T,i} > 20$ GeV, summing only over charged particles in the region $0 < \eta < 2$ with $p_T > 0.5$ GeV, with an additional constraint that there is no charged particle in this region with $p_T > 3$ GeV.

interval of x_{Pom} from 0.0018 to 0.005 (i.e. $\Delta \ln(x_{pom})$ interval equal to 1).[9]

Our results are presented in Figs. 3 and 4. To further suppress the background we impose the following set of experimental selection criteria that look realistic for the present ATLAS and CMS detectors. We exclude the very low p_T particles and consider only the secondary hadrons with transverse momentum $p_T > 0.5$ GeV produced within the $0 < \eta < 2$ rapidity interval, as shown in Fig. 2. We select the events for which the total transverse energy of the charged secondaries (with $p_T > 0.5$ GeV and $0 < \eta < 2$)[10] is

[9]Note that in this region the dependence of single dissociation cross-section $d\sigma/d \ln(1/x_{Pom})$ is practically flat as is shown in [25, 47, 48].

[10]We shifted the η interval in the direction opposite to the LRG (or the leading proton which has the negative rapidity) in order not to have gluons with too large x (where the gluon density rapidly decreases with increasing x) from the pomeron PDF. Recall that for
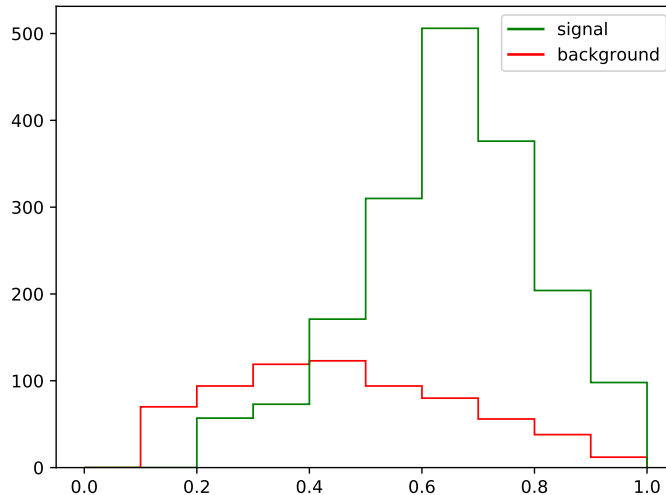
16

Figure 4: Distribution over the transverse sphericity S_T, Eq. (8), of the charged hadrons produced in the events with the instanton (green) in comparison with the expected background (red). Number of events is normalised to the integrated luminosity $L = 1\text{pb}^{-1}$ and $\Delta \ln(x_{Pom}) = 1$ interval. The event selection criteria used are the same as those described in Fig. 3 and we also required that the number of charged tracks in the selected region is $N_{ch} > 20$ and no charged particles present with $p_T > 3$ GeV.

$\sum_i E_{T,i} > 20$ GeV and the number of corresponding charged tracks $N_{ch} > 20$. We also demand that there is no charged particle in this region with $p_T > 3$ GeV.

As is seen in Fig. 4 after the proposed cuts the instanton signal exceeds the background by a factor of over 2.5 and for $S_T > 0.5$ the signal to background ratio S/B is even higher. Notably, in the $N_{ch} > 20$ region the expected cross-section is still rather large ($\sim$ few nb). This allows one to observe the instanton production in low luminosity runs without pile-up problems.

The sphericity distribution is shown in Fig. 4. It is clearly seen that while the background sphericity falls steeply for $S_T > 0.5$ the instanton signal is

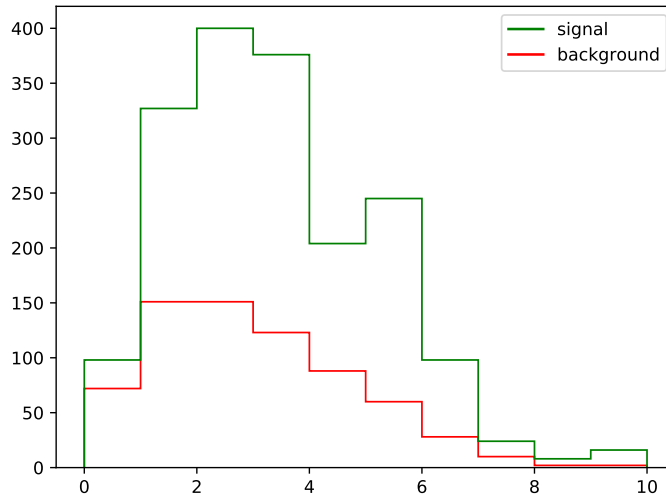$x_{Pom} = 0.003$ the energy of the 'incoming' pomeron is 21 GeV only.

Figure 5: Distribution over the number of neutral kaons produced in the events with the instanton (green) in comparison with the expected backgrond (red). The selection criteria used are the same as those described in Fig. 4.

mainly concentrated at $S_T > 0.5$. For $S_T > 0.8$ the expected instanton contribution is a factor of 6 greater than the background.

Finally, Fig. 5 shows the distribution over the number of neutral kaons. [11] The selection criteria used are the same as those described in Fig. 4. As expected the kaon multiplicity is larger in the events containing the instanton and for $N_{K^0} > 5$ the S/B ratio is about 4.

7   Discussion

The possibility of direct experimental observation of QCD instantons at hadron colliders has recently attracted a fair amount of attention [14, 15, 49]. The authors of [15] evaluated the sensitivity of the LHC and Tevatron high- and low-luminosity runs, and [49] obtained a first limit based on existing Minimum Bias data.

---

[11]This can be observed via the $(K^0)_s \to \pi^+\pi^-$ decay.

18

Extraction of the instanton signal on top of the underlying event at the LHC, not relying on events with large rapidity gaps, is a challenging task. One problem, not considered in [49], is how to select in the experiment the events corresponding to the chosen M_{inst} interval. It is impossible to distinguish the jet emitted by the instanton from the jet created during the parton showering or due to the presence of a perturbative QCD multi-jet 'hedgehog' contribution (the latter is another problem that has not been addressed until now).

The idea to observe instantons in the pomeron-induced process, namely in the central exclusive production,

$$pp \; \to \; p \; + \; X \; + \; p \tag{19}$$

was first put forward in [50] (see also [51]). This was prompted by the reported UA8 observation [52] of the large enhancement in the pomeron-pomeron cross-section at invariant masses $2 < M < 5$ GeV with roughly isotropic distribution of secondaries. Unfortunately, we (present authors) do not have theoretical control over such low-mass instantons, or for that matter other non-perturbative contributions in the infrared. In these settings, there is no external mass parameter and it is not clear how to distinguish instanton production from the background or, for example, from the glueball production. On the other hand searching for a larger-mass instanton in pomeron-pomeron collisions has no advantage in comparison with instanton production in events with one LRG, but in the case of pomeron-pomeron collisions the expected cross-section is much smaller.

7.1   Other instanton production sub-processes

Up to now we were only concentrating on the 2-gluon initiated process (3), but one should also consider other quark, anti-quark and gluon initiated

19

2-parton processes, such as,

$$g + u_L \quad \rightarrow \quad n_g \times g \, + \, u_R + \sum_{f=1}^{N_f - 1} \left(q_{Rf} + \bar{q}_{Lf} \right), \tag{20}$$

$$u_L + \bar{u}_R \quad \rightarrow \quad n_g \times g + \sum_{f=1}^{N_f - 1} \left(q_{Rf} + \bar{q}_{Lf} \right), \tag{21}$$

$$u_L + d_L \quad \rightarrow \quad n_g \times g \, + \, u_R + d_R + \sum_{f=1}^{N_f - 2} \left(q_{Rf} + \bar{q}_{Lf} \right), \tag{22}$$

and also include the contributions from multi-parton initial states.

We first consider the 2-parton initiated processes. Note that there is no interference between all these sub-processes since the fermion content of the external states in (3),(20)-(22) is different. Thus, the total contribution comes from adding the individual cross-sections from these processes, in other words, summing over the integrals (18) with the appropriate choice of pdfs for each of the partons in the initial state. Since each of these contributions is manifestly positive, our already computed contribution from the gluon fusion process (3) cannot be reduced. It is also clear that one cannot expect any sufficient enhancement to it from accounting for the additional channels (20)-(22). This is because for the parton-level cross-section most of the expression in (10), in particular its exponent, remains the same;[12] only the four field insertions for the external states vary. On the other hand, as we have seen, the dominant contributions to hadronic cross-sections come from the low-x region, and as a result, our gluon fusion instanton sub-process is expected to be the dominant one.

Next, we would like to discuss the effects of multi-parton initial states in the instanton production. To do this we would like to distinguish between the two cases: one, where multi-partons entering the instanton have originated from just the two parent partons, and the second case, where the multi-parton initial state has a genuine multi-parton origin, with all 3 or 4 partons being emitted from the proton and/or the pomeron.

---

[12]Up to now we have only included the initial-state corrections arising from the high-energy limit of the gluon propagator in the instanton background, but as was shown in [53], the same result (13) is expected to hold also for fermions in the initial state.

The first case, where the multi-partons in the initial state can be traced to just two parent partons is already accounted for by the resummed quantum corrections from the initial states. Such effects are precisely what is included into the initial-initial state and the initial-final state propagators in the instanton background computed in [29]. Our approach takes into account the initial-initial (i.e. hard-hard) quantum effects by explicitly including the Mueller form-factor term (13). The initial-final state (or hard-soft interactions) were not directly included in our approach,[13] however, the form-factor arising from all such quantum corrections is of the same generic exponential form [29],

$$\exp\Big(-\frac{\alpha_s(\mu_r)}{16\pi}\,\rho^2 E^2 \sum_{i,j} a_{ij}\log a_{ij}\Big), \quad \text{where} \quad a_{ij} := p_i \cdot p_j/E^2\,, \qquad (23)$$

as the initial-initial state form-factor in (13). Hence we do not expect a significant difference in the final result from the inclusion of these effects.

The second case corresponds to *genuine* multi-parton initial states, and it is accounted for by adding the contribution to the total cross-section from the integrals of the type (18), now with multiple pdfs, one for each parton in the initial state. Like in the two-particle case, discussed earlier, this is a manifestly positive contribution that cannot destructively interfere with our two-gluon contribution. In summary, we expect that a more careful inclusion of all instanton production sub-processes could only enhance the gluon fusion contribution (and only moderately).

7.2 Theory uncertainties

Note that all the present calculations should not be considered as the precise theoretical predictions. There are a number of uncertainties.

First of all, one could expect sizeable corrections to the assumed factorization of instanton and anti-instanton collective coordinate integration measure in the forward elastic scattering amplitude (10), which strictly holds only at infinitely large inter-instanton separations $R^2/(\rho\bar\rho) \gg 1$. At finite separations, the integration measure was shown in [27] to satisfy,

$$d\mu_{I\bar I} = d\mu_I\, d\mu_{\bar I}\left(1 + \mathcal{O}\left(\frac{1}{z^2}\right)\right), \qquad (24)$$

_____

[13]This is done to avoid double-counting, since the radiative exchanges involving final-state partons are already accounted for by the optical theorem.

where z is given by (11). In our calculation the mean value of R/ρ was $\simeq 1.55$ at all energies, which corresponds to $z \simeq 4.16$, or $1/z^2 \simeq 0.058$ which is a re-assuringly small value to be optimistic about the validity of the approximate factorization of instanton integration measures (and thus the factorization of the determinants of quadratic fluctuation operators in the instanton–anti-instanton background).

Hence, in terms of the conformal z^2 variable the individual instanton and the anti-instanton are reasonably well-separated. For this reason, we are similarly confident about the validity of the instanton–anti-instanton action expression (12) that was computed for a particular exactly-solvable model [27, 28] of the instanton-anti-instanton valley configuration. What is more difficult to estimate, however, is the role played by the unknown higher-order perturbative corrections to the re-summed quantum exchanges from the initial states in (13).

Furthermore, there is a rather large theoretical uncertainty in evaluation of the gap survival factor S^2, which also depends on the details of the particular subprocess (see [24]). Therefore we prefer to use the experimental value measured in diffractive dijet production[45, 46]. We evaluate the corresponding uncertainty as $\pm 50\%$.

We should also note a potentially strong dependence of the predicted cross-section on the values of the renormalization, μ_R, and factorization, μ_F, scales. In particular, it was found in [54] that replacing the natural scale $\mu_F = 1/\rho$ by the value of $\mu_F = M_{\text{inst}}$ enhances the instanton production cross-section for instantons of mass larger than $M_{\text{inst}} = 50$ GeV computed in [14] by approximately a factor of five.

Besides this, as we have already noted, the present calculations are based on the simplest $gg \rightarrow Instanton$ subprocess neglecting the possibility to produce the instanton in collision with quarks or with a pair of gluons, like $g + gg \rightarrow Instanton$ and so on. Based on our earlier discussion in Section 7.1, we consider it unlikely that these new subprocesses would change the qualitative features of the expected signal, but they may enlarge the final cross-section.

8   Conclusions

We propose to search for the QCD instantons at the LHC in events with Large Rapidity Gaps and in this paper we carried out the first preliminary investigation of this search strategy. These LRG events are selected either

by detecting the forward leading proton with x_L very close to 1 or by observing no hadron activity in the forward calorimeter. We discussed the main sources of background for the low and the high mass instantons and showed that background for the low mass instantons, which comes mainly from multiple parton interactions, is effectively suppressed in the LRG events by the small gap survival factor $S^2 \leq 0.1$. This allowed us to find the kinematical domain where the signal from $M_{\text{inst}} \sim 20 - 60$ GeV instantons reliably exceeds background.

Even with these rather strong cuts in place, the expected instanton cross-section remains sufficiently large ($\sim$ few nb) to effectively produce and probe QCD instantons at the LHC, at low luminosity runs, avoiding pile-up problems.

Acknowledgments

References

[1] A. A. Belavin, A. M. Polyakov, A. S. Schwartz and Y. S. Tyupkin, Phys. Lett. **59B** (1975) 85.

[2] G. 't Hooft, Phys. Rev. D **14** (1976) 343, Erratum: [Phys. Rev. D **18** (1978) 2199].

[3] C. G. Callan, Jr., R. F. Dashen and D. J. Gross, Phys. Lett. **63B** (1976) 334.

[4] R. Jackiw and C. Rebbi, Phys. Rev. Lett. **37** (1976) 172.

[5] G. 't Hooft, Phys. Rept. **142** (1986) 357.

[6] C. G. Callan, Jr., R. F. Dashen and D. J. Gross, Phys. Rev. D **17** (1978) 2717.

[7] V. A. Novikov, M. A. Shifman, A. I. Vainshtein and V. I. Zakharov, Nucl. Phys. B **191** (1981) 301.

[8] E. V. Shuryak, Nucl. Phys. B **203** (1982) 116.

[9] D. Diakonov and V. Y. Petrov, Phys. Lett. **147B** (1984) 351; Nucl. Phys. B **272** (1986) 457.

[10] T. Schäfer and E. V. Shuryak, Rev. Mod. Phys. **70** (1998) 323 hep-ph/9610451.

[11] A. Hasenfratz and C. Nieter, Phys. Lett. B **439** (1998) 366 hep-lat/9806026.

[12] T. A. DeGrand, A. Hasenfratz and T. G. Kovacs, Nucl. Phys. B **505** (1997) 417 hep-lat/9705009.

[13] D. A. Smith *et al.* [UKQCD Collaboration], Phys. Rev. D **58** (1998) 014505 hep-lat/9801008.

[14] V. V. Khoze, F. Krauss and M. Schott, JHEP **2004** (2020) 201 arXiv:1911.09726 [hep-ph].

[15] V. V. Khoze, D. L. Milne and M. Spannowsky, Phys. Rev. D **103** (2021) no.1, 014017 arXiv:2010.02287 [hep-ph].

[16] I. I. Balitsky and V. M. Braun, Phys. Lett. B **314** (1993) 237 hep-ph/9305269.

[17] S. Moch, A. Ringwald and F. Schrempp, Nucl. Phys. B **507** (1997) 134 hep-ph/9609445.

[18] A. Ringwald and F. Schrempp, Phys. Lett. B **438** (1998) 217 hep-ph/9806528.

[19] C. Adloff *et al.* [H1 Collaboration], Eur. Phys. J. C **25** (2002) 495 hep-ex/0205078.

[20] S. Chekanov *et al.* [ZEUS Collaboration], Eur. Phys. J. C **34** (2004) 255 hep-ex/0312048.

[21] M. Aaboud *et al.* [ATLAS Collaboration], Phys. Lett. B **790** (2019) 595 arXiv:1811.11094 [hep-ex].

[22] M. Sas and J. Schoppink, arXiv:2101.12367 [hep-ph].

[23] A. Buckley, J. Butterworth, S. Gieseke, D. Grellscheid, S. Hoche, H. Hoeth, F. Krauss, L. Lonnblad, E. Nurse and P. Richardson, *et al.* Phys. Rept. **504** (2011), 145-233 arXiv:1101.2599 [hep-ph].

[24] V. A. Khoze, A. D. Martin and M. G. Ryskin, J. Phys. G **45** (2018) no.5, 053002 arXiv:1710.11505 [hep-ph].

[25] V. A. Khoze, A. D. Martin and M. G. Ryskin, Eur. Phys. J. C **81** (2021) no.2, 175 arXiv:2012.07967 [hep-ph].

[26] I. I. Balitsky and M. G. Ryskin, Phys. Atom. Nucl. **56**, 1106 (1993) [Yad. Fiz. **56N8**, 196 (1993)]; Phys. Lett. B **296** (1992) 185.

[27] A. V. Yung, Nucl. Phys. B **297** (1988) 47.

[28] V. V. Khoze and A. Ringwald, Phys. Lett. B **259** (1991) 106; "Valley trajectories in gauge theories," CERN-TH-6082-91 (1991).

[29] A. H. Mueller, Nucl. Phys. B **348** (1991) 310; Nucl. Phys. B **353** (1991) 44.

[30] A. Donnachie and P. V. Landshoff, Nucl. Phys. B **231** (1984) 189.

[31] M. Beneke and M. Jamin, JHEP **0809** (2008) 044 arXiv:0806.3156 [hep-ph].

[32] G. Abbas, B. Ananthanarayan, I. Caprini and J. Fischer, Phys. Rev. D **87** (2013) no.1, 014008 arXiv:1211.4316 [hep-ph].

[33] S. Schael *et al.* [ALEPH Collaboration], Phys. Rept. **421** (2005) 191 hep-ex/0506072.

[34] K. Ackerstaff *et al.* [OPAL Collaboration], Eur. Phys. J. C **7** (1999) 571 hep-ex/9808019.

[35] A. M. Badalian and V. L. Morgunov, Phys. Rev. D **60** (1999) 116008 hep-ph/9901430.

[36] P. Virtanen, R. Gommers, T. E. Oliphant, M. Haberland, T. Reddy, D. Cournapeau, E. Burovski, P. Peterson, W. Weckesser and J. Bright, *et al.* Nature Meth. **17** (2020), 261 arXiv:1907.10121 [cs.MS].

[37] R. Kleiss, W. J. Stirling and S. D. Ellis, Comput. Phys. Commun. **40** (1986), 359

[38] T. Sjöstrand, S. Ask, J. R. Christiansen, R. Corke, N. Desai, P. Ilten, S. Mrenna, S. Prestel, C. O. Rasmussen and P. Z. Skands, Comput. Phys. Commun. **191** (2015), 159-177 arXiv:1410.3012 [hep-ph].

[39] A. Buckley, J. Ferrando, S. Lloyd, K. Nordström, B. Page, M. Rüfenacht, M. Schönherr and G. Watt, Eur. Phys. J. C **75** (2015), 132 arXiv:1412.7420 [hep-ph].

[40] V. Bertone *et al.* [NNPDF], SciPost Phys. **5** (2018) no.1, 008 arXiv:1712.07053 [hep-ph].

[41] A. V. Manohar, P. Nason, G. P. Salam and G. Zanderighi, JHEP **12** (2017), 046 arXiv:1708.01256 [hep-ph].

[42] A. Manohar, P. Nason, G. P. Salam and G. Zanderighi, Phys. Rev. Lett. **117** (2016) no.24, 242002 arXiv:1607.04266 [hep-ph].

[43] A. Aktas *et al.* [H1 Collaboration], Eur. Phys. J. C **48** (2006) 715 hep-ex/0606004.

[44] M. Botje, Comput. Phys. Commun. **182** (2011) 490 arXiv:1005.1481 [hep-ph].

[45] A. M. Sirunyan *et al.* [CMS and TOTEM Collaborations], Eur. Phys. J. C **80** (2020) no.12, 1164 arXiv:2002.12146 [hep-ex].

[46] G. Aad *et al.* [ATLAS Collaboration], Phys. Lett. B **754** (2016) 214 arXiv:1511.00502 [hep-ex].

[47] G. Aad *et al.* [ATLAS Collaboration], JHEP **2002** (2020) 042 Erratum: [JHEP **2010** (2020) 182] arXiv:1911.00453 [hep-ex].

[48] V. Khachatryan *et al.* [CMS Collaboration], Phys. Rev. D **92** (2015) no.1, 012003 arXiv:1503.08689 [hep-ex].

[49] S. Amoroso, D. Kar and M. Schott, arXiv:2012.09120 [hep-ph].

[50] E. Shuryak and I. Zahed, Phys. Rev. D **68** (2003), 034001 arXiv:hep-ph/0302231 [hep-ph].

[51] E. Shuryak and I. Zahed, arXiv:2102.00256 [hep-ph].

[52] A. Brandt *et al.* [UA8], Eur. Phys. J. C **25** (2002), 361-377 arXiv:hep-ex/0205037 [hep-ex].

[53] V. V. Khoze and D. L. Milne, Int. J. Mod. Phys. A **36** (2021) no.05, 2150032 arXiv:2011.07167 [hep-ph].

[54] M. Mangano, arXiv:2101.02719 [hep-ph].